# A Numerical Study of Storm Surges and Tides, with Application to the North Queensland Coast

YONG MING TANG,*,+ ROGER GRIMSHAW,+ BRIAN SANDERSON,* AND GREG HOLLAND*

*Bureau of Meteorology Research Centre, Melbourne, Victoria, Australia
+Department of Mathematics, Monash University, Clayton, Victoria, Australia

(Manuscript received 2 May 1995, in final form 14 May 1996)

ABSTRACT

A two-dimensional numerical model of the shallow-water equations, with a modified Orlanski-type radiation boundary condition, is applied to study storm surges and tides on the North Queensland coast. The numerical simulations show that with the tides included in the storm surge model the sea level elevation is generally lower than if we simply add the astronomical tides to the surge. This has been previously observed and has been commonly explained as a nonlinear interaction between the storm surge and the tides. The authors demonstrate that this effect is due to the quadratic bottom friction law. Analysis of the important dynamical processes yields a simple rule to estimate the total sea level due to the combined effects of a storm surge and tide.

## 1. Introduction

Numerical modeling of the circulation in the coastal ocean is now well developed and has been applied to the study of tides, currents, and wind-driven events, such as storm surges, in shallow coastal seas (Prandle and Wolf 1978; Fandry 1981; Heaps 1983; Johns et al. 1985; Proctor and Wolf 1990; O'Connor 1991; Davies and Jones 1992; Verboom et al. 1992; Flather 1994; Das 1994). Most attention has been paid to the modeling of individual processes, such as tides alone, or the storm surge generated by a tropical cyclone, and comparatively little is known about the dynamical interactions when two, or more, processes can occur together. Further, usually those studies that do simulate storm surges in the presence of tides do not attempt a detailed analysis of these dynamical interactions (notable exceptions are Prandle and Wolf 1978; Heaps 1983; Johns et al. 1985; Proctor and Wolf 1990; Das 1994). Here we are concerned with the numerical simulation of storm surges and tides simultaneously and an examination of the dynamical causes of the interaction between them. Our study is motivated by the situation in the Mackay region of the North Queensland coast (NQC), which while being prone to storm surges generated by tropical cyclones (Whittingham 1958) is also a region of high tides (Middleton et al. 1984; Andrews and Bode 1988).

A simple approach to predicting the total coastal sea level might be to numerically calculate the storm surge alone, due to a specified tropical cyclone forcing, and then to linearly superpose on this the astronomical tide, as obtained from tide tables or predicted from a separate numerical calculation. It is widely known, however, that such a linear superposition is not strictly correct due to nonlinear interactions between the storm surge and tide and tends to usually overestimate the total coastal sea level elevation (e.g., Prandle and Wolf 1978; Heaps 1983; Johns et al. 1985; Proctor and Wolf 1990; Das 1994). We are not aware of any studies (other than those noted below) that probe the cause of this nonlinear interaction and the consequences. Hence, it is our purpose here to provide such a study by numerical simulations of storm surges and tides in the Mackay region of NQC. We will demonstrate that the nonlinear interaction between a typical storm surge and the tide is predominantly due to the quadratic bottom friction law and is not due to the nonlinear advection terms in the momentum equations or to the nonlinear terms in the equation for the conservation of mass. Further, this interaction generally tends to reduce the sea level below that due to the superposition of the astronomical tide on the storm surge. The dynamical reasons for the above reduction are investigated, culminating in a simple dimensional argument that gives a nonlinear rule for adding the astronomical tide to the storm surge. We note that Prandle and Wolf (1978) (see also Heaps 1983) in a one-dimensional numerical model of the storm surge and tide interaction in the Thames estuary identified the quadratic bottom friction as the principal interaction mechanism, but their analysis method differs from ours and they did not obtain the simple dimensional explanation that we will provide. Also, Proctor and Wolf (1990) carried out an energy budget anal-

*Corresponding author address:* Dr. Yong Ming Tang, Department of Mathematics, Monash University, Clayton, Vic 3168, Australia.

ysis in a hindcast of a North Sea storm surge and also identified quadratic bottom friction as the principle interaction mechanism, but again they did not obtain our explanation.

Numerical models for storm surges, and/or tides, have included both two- and three-dimensional models. Both two-dimensional and three-dimensional models use the shallow-water equations with wind stress driving terms and tidal forcing at the open ocean boundaries. Two-dimensional models often parametrize bottom friction as a quadratic function of the vertically averaged current, although there are various techniques available to modify this and provide a closer relation with the frictional parametrization of three-dimensional models (e.g., Davies and Jones 1993). Three-dimensional models usually consider homogeneous fluids but allow for frictionally induced vertically sheared currents that have the potential to enable a more sophisticated estimation of bottom stress (Blumberg and Mellor 1987). Here, however, we use a conventional two-dimensional model since our main concern is with the prediction of the coastal sea level, and it is well known that two-dimensional models are adequate for the calculation of the sea level elevation and the depth-averaged currents (Proctor and Flather 1989; O'Connor 1991; Das 1994). Further, although it is possible that more sophisticated frictional parametrizations than the one we use [see (2.8)] could lead to some difference in detail to our results, we contend that the simplicity of our dimensional argument points to the robust nature of our general conclusions.

In section 2 we describe the formulation of the governing equations and our numerical scheme. The tropical cyclone wind stress forcing and the tidal forcing at the models open boundaries are described in section 3. In section 4 we present numerical results. A discussion of the dynamics underlying our numerical results and a simple dimensional argument follow in section 5.

## 2. Governing equations and numerical scheme

In standard notation, the two-dimensional barotropic shallow water equations are

$$u_t + uu_x + vu_y - fv + g\zeta_x = \frac{\tau_W^{(x)}}{\rho H} - \frac{\tau_B^{(x)}}{\rho H} - \frac{P_{Ax}}{\rho} \quad (2.1)$$

$$v_t + uv_x + vv_y + fu + g\zeta_y = \frac{\tau_W^{(y)}}{\rho H} - \frac{\tau_B^{(y)}}{\rho H} - \frac{P_{Ay}}{\rho} \quad (2.2)$$

$$\zeta_t + (Hu)_x + (Hv)_y = 0, \quad (2.3)$$

where $H = h + \zeta$, $h(x, y)$ is the undisturbed water depth, $\zeta$ is the surface elevation, $(u, v)$ are the velocity components in the alongshelf $(x)$ and cross-shelf $(y)$ directions, $f$ is the Coriolis parameter, $g$ is gravitational acceleration, $\rho$ is water density, $\tau_W^{(x,y)}$ are the wind stress components, $\tau_B^{(x,y)}$ are the bottom stress components, and $P_A$ is the atmospheric pressure. The wind stress $\tau_W^{(x,y)}$ is specified in section 3.

The tidal forcing is specified at the open boundaries. Let $\zeta_T$ be the tidal component at the boundaries, which is the sum of the four major tidal constituents ($M_2$, $S_2$, $K_1$, $O_1$) and is discussed further in section 3. Denote $\tilde{\zeta}$ as the difference between the sea level $\zeta$ and the tidal component, so that $\tilde{\zeta} = \zeta - \zeta_T$. At the open boundaries we apply a suitable radiation condition to $\tilde{\zeta}$. Here we use a modified Orlanski radiation condition (Tang and Grimshaw 1996a) suitable for storm surge simulations. Thus, if $\tilde{\zeta}_B^n$ is the value of $\tilde{\zeta}$ at the $n$th time step and the boundary point $B$, then

$$\tilde{\zeta}_B^{n+1} = \tilde{\zeta}_{B-1}^n + s(\tilde{\zeta}_B^n - \tilde{\zeta}_{B-1}^{n+1}), \quad (2.4)$$

where the value of $s$ in (2.4) is given by

$$s = \begin{cases} \hat{s}, & \text{if } 0 < \hat{s} < 1 \\ 1, & \text{if } |\hat{s}| \geq 1 \\ 0, & \text{if } -1 < \hat{s} \leq 0 \end{cases} \quad (2.5)$$

and $\hat{s}$ is determined implicitly by

$$\hat{s} = \frac{\tilde{\zeta}_{B-1}^n - \tilde{\zeta}_{B-2}^{n-1}}{\tilde{\zeta}_{B-1}^{n-1} - \tilde{\zeta}_{B-2}^n}. \quad (2.6)$$

The second and third conditions in (2.5) are imposed to satisfy stability.

If the coastal boundary is treated as a rigid wall, then the boundary condition is

$$hu_n = 0, \quad (2.7)$$

where $u_n$ is the velocity component normal to the boundary. An alternative, which is used here, is to impose sufficiently large friction over the land region to reduce the velocity field there to zero. This has the advantage of allowing us to use a rectangular grid and perhaps allowing some water to cross the initial land–sea boundary. It is a particularly useful device here, when the coastline is very irregular, as the representation of an irregular coastline by a rectangular grid can cause numerical difficulties (Das 1994). The inundation aspect of our land–sea boundary condition is currently under investigation. But since this is not of immediate concern here, we shall not discuss it further.

The usual quadratic law is used for bottom friction,

$$\tau_B^{(x,y)} = C_D q(u, v), \quad (2.8)$$

where $q = \sqrt{u^2 + v^2}$, and we choose $C_D = 2.0 \times 10^{-3}$. For purposes of comparison, we also consider the linear bottom friction law

$$\tau_B^{(x,y)} = \alpha(u, v), \quad (2.9)$$

where $\alpha = 1.2 \times 10^{-1}$ cm s$^{-1}$ (e.g., Csanady 1984).

The numerical model for the discretized equations is described in Tang et al. (1990a,b) and Tang (1994). Here, for convenience, we give a brief outline of the scheme. The discretized variables are evaluated on an Arakawa B-grid where $\zeta$ is evaluated at the grid points and $u$, $v$ are evaluated at the center of each grid. To

step forward in time the momentum equations are first rewritten in the form

$$Q_t + ifQ = F, \tag{2.10}$$

where $Q = H(u + iv)$ is the complex depth-integrated transport variable, and $F$ is a combination of the nonlinear terms, the pressure gradient, and the forcing term. Integration of (2.10) from $t - \Delta t$ to $t$ and use of the trapezoidal rule of integration gives

$$Q(t) = Q(t - \Delta t)e^{-if\Delta t} + \frac{1}{2}\{F(t) + F(t - \Delta t)e^{-if\Delta t}\}. \tag{2.11}$$

The nonlinear terms in $F$ are put in conservation form and are then discretized by applying Green's integral formula to each grid. We then use the "splitting current" method of Tang et al. (1990a,b; see also Tang 1994) to rearrange (2.11) into the form

$$Q = -A(\zeta_x + i\zeta_y) - (S + iT), \tag{2.12}$$

where at the time step $t$, the real variables $A$, $S$, and $T$ are known in terms of $Q$ at time $t - \Delta t$ and other terms, including the nonlinear terms and the tropical cyclone forcing terms. Substitution of (2.12) in (2.3) then gives

$$\zeta_t = (A\zeta_x)_x + (A\zeta_y)_y + S_x + T_y. \tag{2.13}$$

After incorporating the boundary conditions, (2.13) is integrated forward in time using a Crank–Nicholson scheme.

## 3. Atmospheric and tidal forcing

### a. Atmospheric forcing

The expressions given by Holland (1980) are used to model the wind and atmospheric pressure profile for a tropical cyclone. The atmospheric pressure $P_A$ at radius $r$ from the cyclone center is

$$P_A = P_c + (P_n - P_c)\exp[-(r_m/r)^b], \tag{3.1}$$

where $P_c$ is the cyclone center pressure, $P_n$ is the environmental pressure, $r_m$ is the radius of the maximum winds, and $b$ is defined by

$$b = 1.5 + (980 - P_c)/120, \tag{3.2}$$

which provides a scaling on the profile shape.

The symmetric, gradient-level azimuthal wind component at radius $r$ is

$$v = \{b(r_m/r)^b(P_n - P_c)\exp[-(r_m/r)^b]/\rho_a + r^2f^2/4\}^{1/2} - r|f|/2, \tag{3.3}$$

where $\rho_a$ is the air density. A first-order asymmetry of the wind field is formed by adding the cyclone translation speed to the symmetric wind field and rotating the resulting velocity field so that the maximum wind is 70° to the left of the direction of the cyclone motion. Tropical cyclones have a radial inflow that is constructed by rotating the symmetric wind to a constant inflow angle of 25° outside the radius of the maximum wind. The surface wind is then derived using a constant reduction factor of 0.7 (Hubbert et al. 1991).

The wind stresses are obtained from the wind velocity $(U, V)$ by using the quadratic drag law

$$\tau_W^{(x,y)} = c_d\rho_a W(U, V), \tag{3.4}$$

where $W = \sqrt{U^2 + V^2}$ is wind speed and $c_d$ is the drag coefficient. Following Smith and Banke (1975), the drag coefficient is

$$c_d = (0.63 + 0.066W) \times 10^{-3} \tag{3.5}$$

if the wind speed $W$ is less than 25 m s$^{-1}$ and

$$c_d = [2.28 + 0.033(W - 25)] \times 10^{-3} \tag{3.6}$$

if the wind speed $W$ is above 25 m s$^{-1}$ (Frank 1984).

### b. Tidal forcing

The tides of NQC have attracted much attention lately (e.g., Andrews and Bode 1988), but the lack of good quality offshore tidal data has made it difficult to construct good cotidal charts. Nevertheless, the overall structure of the tides in this region is clear. In general there seems to be a dominant semidiurnal tide at the coast, with constituent $M_2$. Here we use the four major tidal constituents ($M_2$, $S_2$, $K_1$, $O_1$), which cover 80% of the tidal amplitude in NQC. Each tidal constituent $\zeta_n$ ($n = 1, 2, 3, 4$) at a given boundary point is expressed as a time series,

$$\zeta_n = \zeta_0 \cos(\sigma t - \phi). \tag{3.7}$$

Here $\zeta_0$ and $\phi$ are the amplitude and the phase lag of the corresponding tidal constituent, provided by Australian National Tidal Facility on a grid with a spacing of 0.25°, and interpolated onto our grid with a spacing of 0.1°.

## 4. Numerical results

First, we consider a simulation using only tidal forcing at the open boundaries with quadratic bottom friction (2.8). The results (not shown here in full) are considered only after sufficient time for the tides to equilibrate to a periodic solution. In Fig. 2a we show the contours of surface elevations at $t = 24$ h. The time series of the surface elevation at some selected locations (Fig. 3a) show that the tides in NQC are mainly semidiurnal. Around Mackay the tidal range reaches 5 m, but in Townsville it is only 3 m. There is a 2–4 h phase difference between Mackay and Townsville. This agrees with the data published in the Australian National Tide Tables (1994). The tidal current is mainly in the cross-shelf direction in the top and center part of the domain, with some flow across the lower

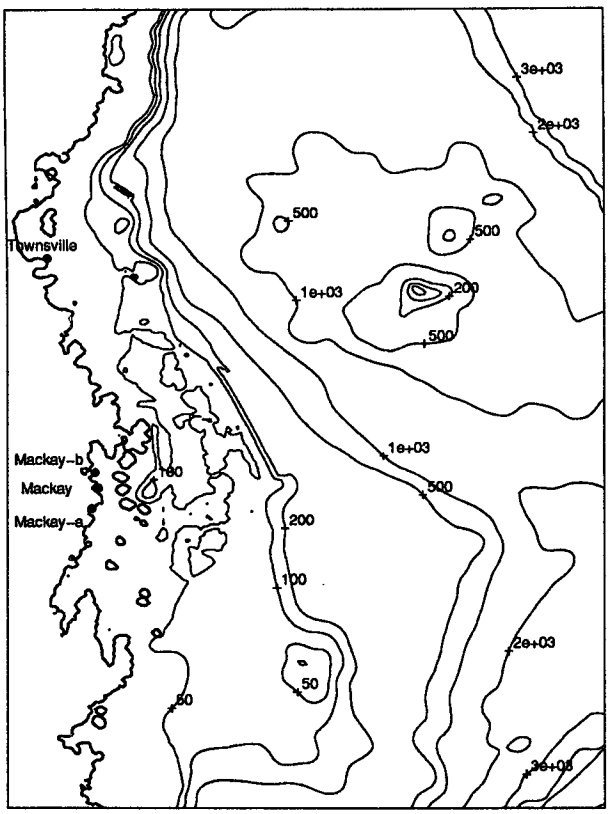


FIG. 1. The computational domain for the north Queensland coast. The region shown is 600 km × 1000 km, and depth contours are in meters.

boundary. The maximum current is offshore from the Mackay region.

The parameter settings for the tropical cyclone model are $P_n$ = 1005 hPa, $P_c$ = 850 hPa, and $r_m$ = 50 km; these are typical values for this region (Lourensz 1981). The cyclone travels southward parallel to the coast with a speed of 20 km $h^{-1}$ and is centered near the shallow water. The cyclone starts in the north and its intensity is ramped up over a 3-h period and subsequently ramped down before it crosses the southern boundary of the model domain. Figure 2b shows the cyclone wind stress field at $t$ = 24 h. Forcing the model with only the cyclone wind stress and pressure results in a storm surge with surface elevations at $t$ = 24 h plotted in Fig. 2c. But a simulation with both cyclone and tidal forcing combined gives the sea surface elevations, again at $t$ = 24 h, plotted in Fig. 2d. Note that in this latter simulation we first establish the tide before introducing the tropical cyclone forcing. As in the pure tidal simulation, we use quadratic bottom friction (2.8) for both the surge and surge plus tide simulations.

To compare these results from the three simulations above we plot time series of the sea level elevation at four locations in Fig. 3. Three of these locations are near Mackay and one near Townsville, as plotted in Fig. 1. In Figs. 3a and 3b we show the sea level elevations for the tides and the storm surge alone respectively. The sea levels are much lower (up to 40% difference in the peak elevations) when the model is forced by the cyclone and the tide combined (Fig. 3c) than if we simply add the sea levels obtained from two simulations forced independently by cyclone and tide (Fig. 3d). The residual difference between the sea level elevations in Figs. 3c and 3d is shown in Fig. 3e.

This phenomenon, demonstrated by the residuals plotted in Fig. 3e, has been observed by many researchers (e.g., Prandle and Wolf 1978; Johns et al. 1985; Das 1994) and has been explained as a nonlinear in-

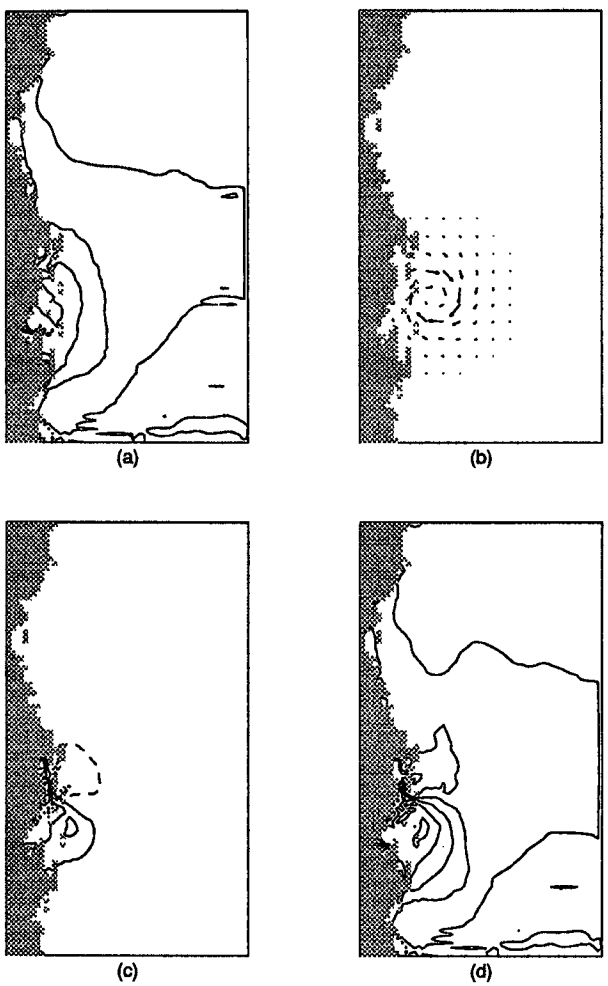


FIG. 2. Numerical results at $t$ = 24 h. (a) Contour plots of sea level elevation produced by tidal forcing alone with contour intervals of 50 cm, (b) tropical cyclone forcing with maximum wind stress forcing of 380 dyn $cm^{-2}$, (c) contour plots of sea level elevation produced by tropical cyclone forcing alone with contour intervals of 50 cm, and (d) contour plots of sea level elevation produced by tropical cyclone forcing and tidal forcing combined with contour intervals of 50 cm.

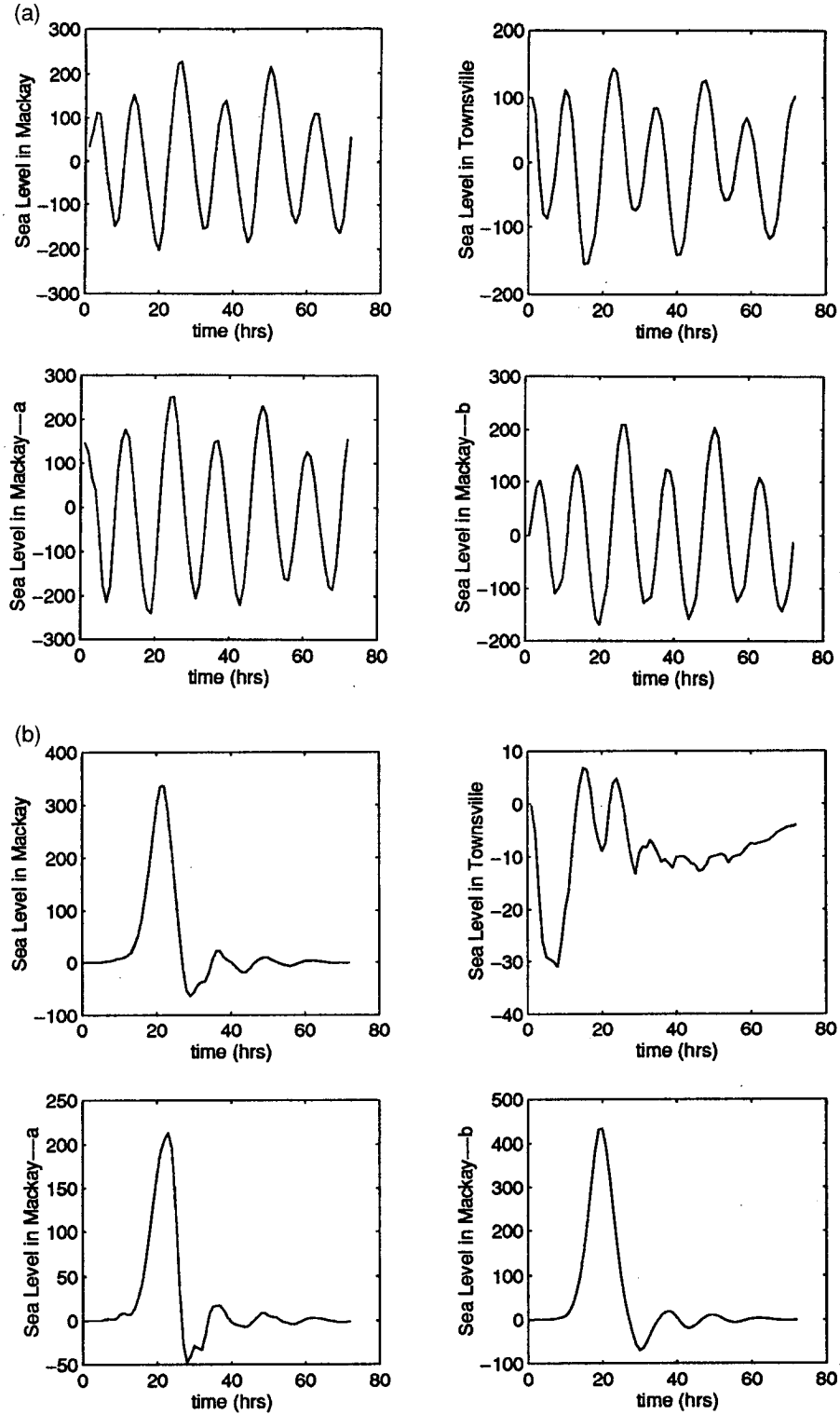


FIG. 3. (a) Sea level elevation (in cm) in three locations near Mackay and Townsville (as shown in Fig. 1) produced by tidal forcing alone, with quadratic bottom friction law. (b) As in (a) but produced by tropical cyclone forcing alone.

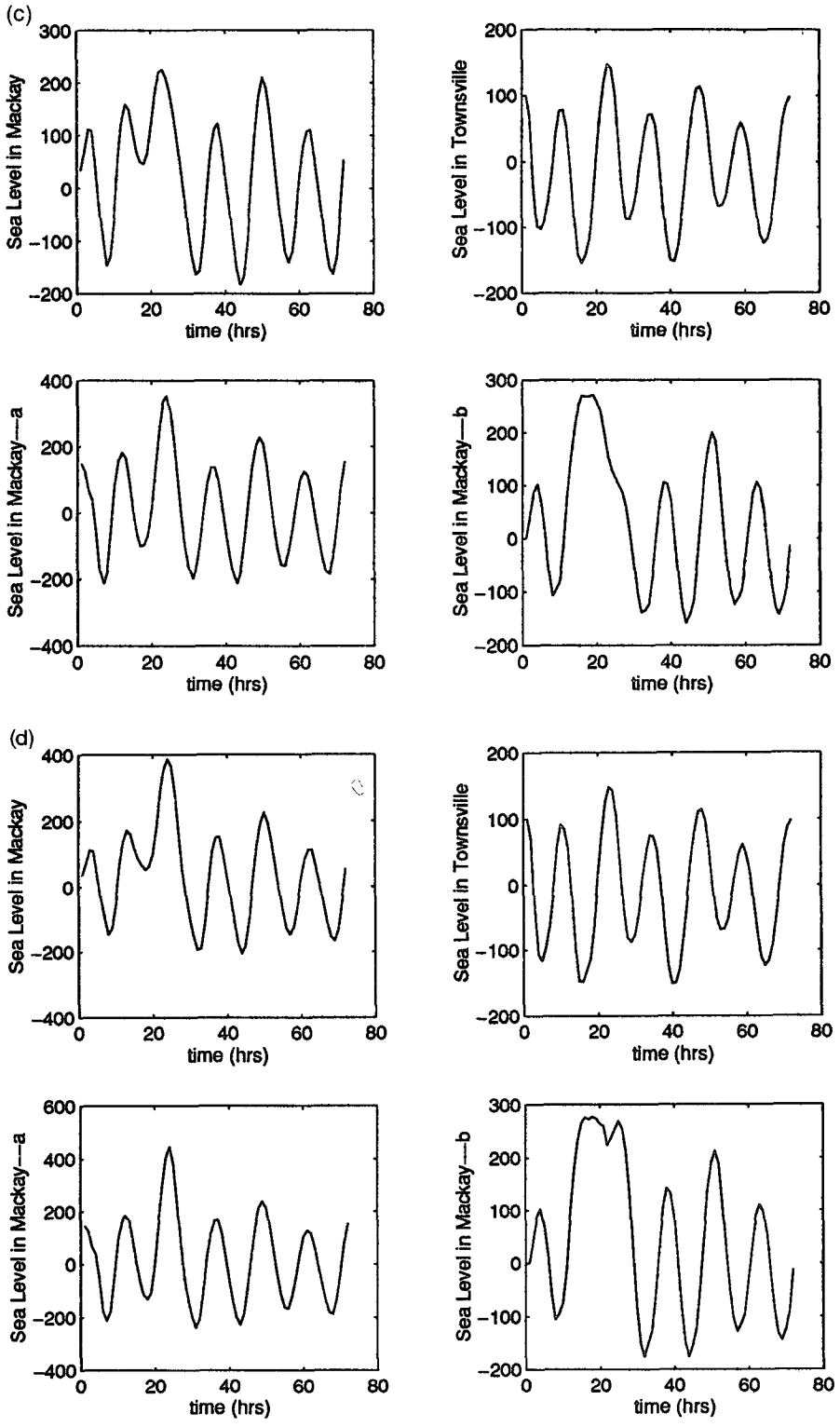


FIG. 3. (*Continued*) (c) As in (a) but produced by tropical cyclone forcing and tidal forcing combined. (d) As in (a) but by adding the tides to the sea level produced by tropical cyclone forcing alone.

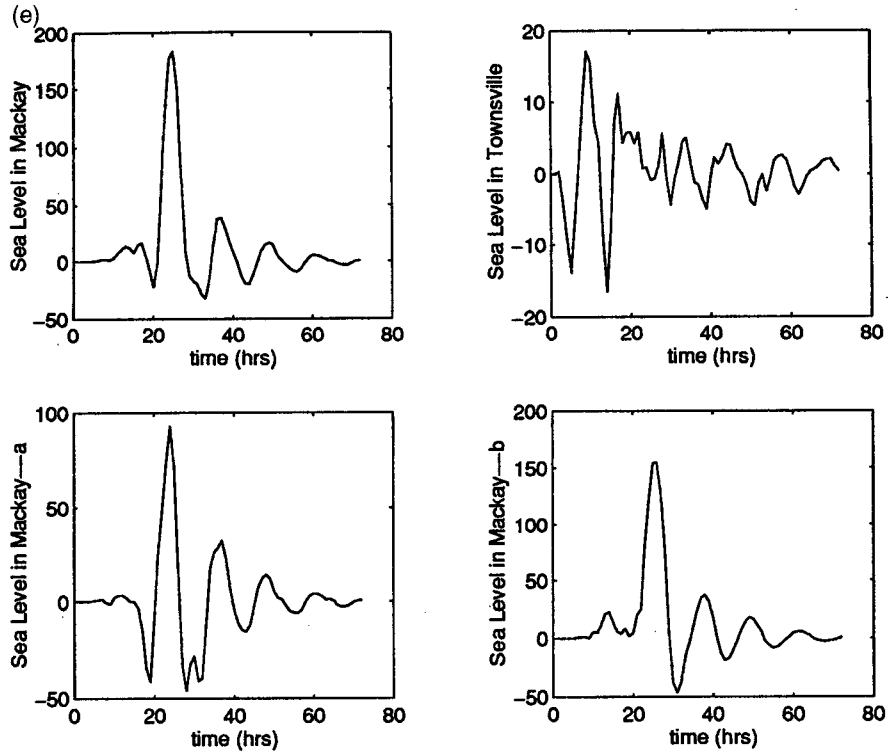


FIG. 3. (*Continued*) (e) As in (a) but the residual of (d) and (c).

teraction between the storm surge and the tide. To determine the origin of this nonlinear interaction, we next simulated the response when we omit all the nonlinear terms on the left-hand side in the equations of motion (2.1) to (2.3) and replace the total depth $H$ by the undisturbed depth $h$ on the right-hand side, but (significantly) retain the quadratic bottom friction law. The result is shown in Fig. 4, which shows the residual, being the counterpart of Fig. 3e. There is no substantial meaningful difference between these figures. Hence the nonlinear interaction between the storm surge and the tides is due to the quadratic bottom friction law. To reinforce this interpretation, we note that the response to either tidal forcing alone or to tropical cyclone forcing alone, with the nonlinear terms on the left-hand side in the equations of motion again omitted (these results are not shown here), is the same as those shown in Figs. 3a and 3b respectively, thus confirming that these nonlinear terms are not significant for either forcing component or for the combined forcing.

Next, with the nonlinear terms on the left-hand side of the equations of motion again omitted and the total depth $H$ replaced by the undisturbed depth $h$ on the right-hand side, we replaced the quadratic bottom friction (2.8) with the linear friction law (2.9) and repeated the above sequence of simulations. The results (see Fig. 5, for the residual) now show that, as expected, the response to a combination of tidal and tropical cyclone forcing is just the linear sum of the response to each forcing component separately.

The conclusion from this sequence of simulations is clear: the nonlinear interaction between the storm surge and the tide is due to the quadratic bottom friction law. The nonlinear advection terms in the momentum equations and the nonlinear terms in the equation for conservation of mass play an insignificant role, consistent with the scaling analysis of Welander (1961). Moreover, the effect of this nonlinear interaction is to reduce the coastal sea level below that obtained by linearly adding the astronomical tide to the storm surge simulation alone. Of course, we have here presented just a single parameter setting, and hence the sequence of simulations was repeated for different parameter settings, as well as for different tropical cyclone strengths and paths. The results (not shown here) are generally very similar with respect to the effect of the quadratic bottom friction to the single case study we have shown here. Further, we have chosen to discuss our results in terms of coastal sea level response, but as our dynamical scaling argument in section 5 suggests, the same conclusions can be drawn from other fields such as the currents.

## 5. Discussion

From our numerical simulations, we conclude that the left-hand side of the equations of motion (2.1) to

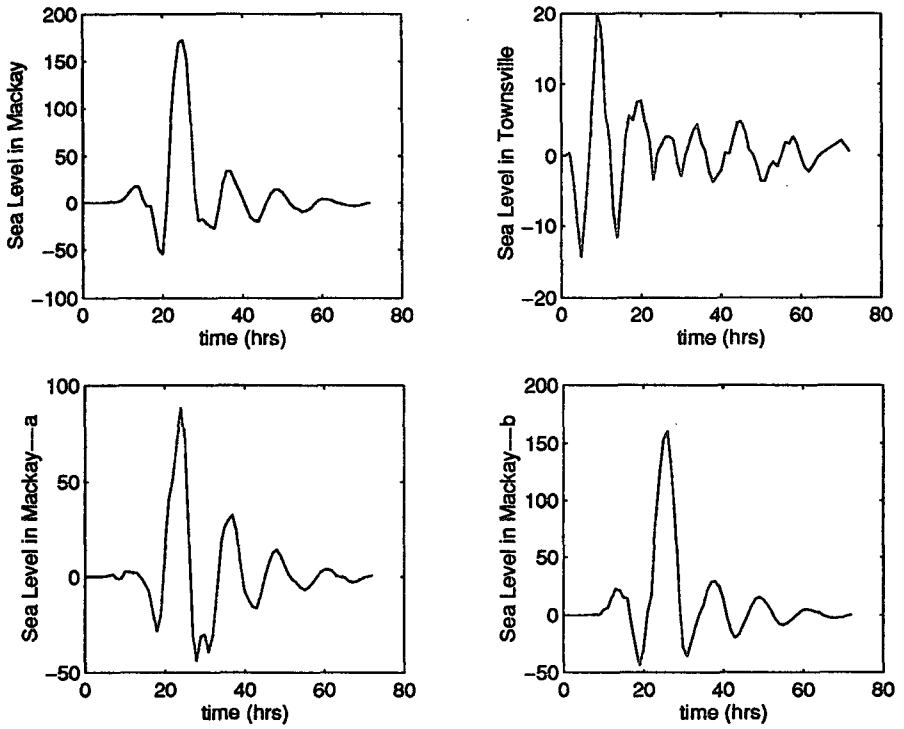


FIG. 4. As in Fig. 3e but without the nonlinear terms on the left-hand side in the equations of motion [(2.1)–(2.3)].

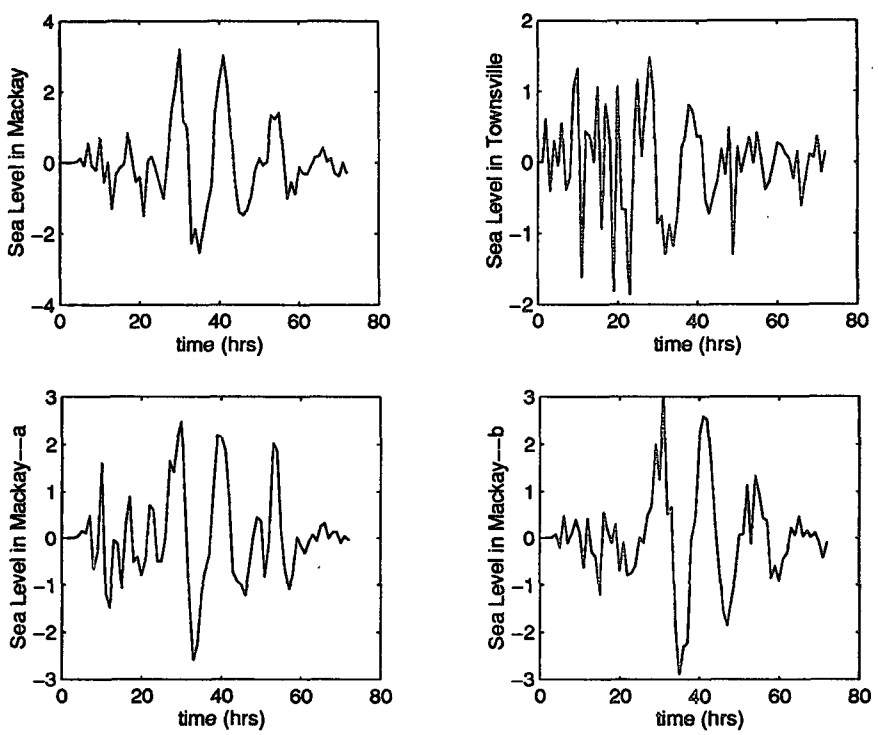


FIG. 5. As Fig. 4 but replacing the quadratic bottom friction law with a linear bottom friction law.

(2.3) can be reduced to a linear system, subjected to a forcing provided here by the tides and tropical cyclones, and controled by quadratic bottom friction. If we schematically represent the forcing by $F$ and the friction by $\tau$, then in a quasi-steady state there will be a balance between these two. Further, for a quadratic bottom friction law we can suppose, again schematically, that $\tau$ is proportional to $\phi^2$, where $\phi$ represents an appropriate scaling magnitude for the physical variables of the system. Then the balance between $F$ and $\tau$ implies that

$$\phi = \sqrt{F}. \tag{5.1}$$

We have considered three different forcing systems here. These are tidal forcing $F_T$ alone, tropical cyclone forcing $F_S$ alone, and the combination of both tidal forcing and tropical cyclone forcing $F_T + F_S$. The corresponding system response can then be represented by $\phi_T$, $\phi_S$, and $\phi_{TS}$, respectively. Since the system is essentially linear, we then have the following relationships:

$$\phi_T = \sqrt{F_T}, \quad \phi_S = \sqrt{F_S},$$

and

$$\phi_{TS} = \sqrt{F_T + F_S}. \tag{5.2}$$

But since

$$\sqrt{F_T + F_S} < \sqrt{F_T} + \sqrt{F_S}, \tag{5.3}$$

which is just an elementary inequality, it follows that

$$\phi_{TS} < \phi_T + \phi_S. \tag{5.4}$$

This simple argument, we believe, serves to demonstrate the robustness of the result that we have obtained here; that is, the nonlinear interaction between the storm surge and tide generally results in a smaller response than would be obtained by simply adding the response when the system is forced by either component alone.

To reinforce this view, suppose we now replace the quadratic bottom friction law with a linear law so that we now have $\tau$ proportional to $\phi$. Repeating the above steps, we get instead

$$\phi_T = F_T, \quad \phi_S = F_S$$

and

$$\phi_{TS} = F_T + F_S, \tag{5.5}$$

so

$$\phi_{TS} = \phi_T + \phi_S. \tag{5.6}$$

As expected, the combined response is just the linear sum of the separate responses.

Since the above argument is only schematic, we now look in more detail at how it relates to the governing equations and boundary conditions described in section 2. For wind stress driven systems the frictional adjustment timescale is (Csanady 1984)

$$t_f = \frac{h}{2\sqrt{\tau_W c_d}}, \tag{5.7}$$

where $\tau_W$ is the wind stress magnitude and $c_d$ is the drag coefficient [see (3.4)]. In shallow water, say $h < 100$ m, this frictional timescale is about 1 h. But, the timescale for the wind forcing is much larger than this, say about 10 h. Further, the inertial period is also about 10 h. Consequently the primary balance in the momentum equation is between the hydrostatic pressure gradient, the wind stress, and bottom friction so that (2.1) and (2.2) reduce to

$$g\zeta_x = \frac{\tau_W^{(x)}}{\rho h} - \frac{\tau_B^{(x)}}{\rho h} - \frac{P_{Ax}}{\rho} \tag{5.8}$$

$$g\zeta_y = \frac{\tau_W^{(y)}}{\rho h} - \frac{\tau_B^{(y)}}{\rho h} - \frac{P_{Ay}}{\rho}, \tag{5.9}$$

where we have omitted the local time acceleration terms, the advective acceleration terms, and the Coriolis terms on the left-hand side and replaced the total depth $H$ by the undisturbed depth $h$ on the right-hand side. The equation for conservation of mass (2.3) is also linearized and becomes

$$\zeta_t + (hu)_x + (hv)_y = 0, \tag{5.10}$$

where we have retained the small term $\zeta_t$ to avoid degeneracy (Sanderson et al. 1995). Essentially, (5.10) establishes that $\zeta$ is linearly related to $u$ and $v$. Note that these reduced equations constitute the quasi-steady hypothesis.

Next, in a conventional manner, we can obtain the corresponding reduced energy equation from (5.8), (5.9), and (5.10). That is,

$$\rho g(hu\eta)_x + \rho g(hv\eta)_y = (u\tau_W^{(x)} + v\tau_W^{(y)}) - \rho C_D q^3, \tag{5.11}$$

where $\eta = \zeta + P_A/g$, and we recall that $q = \sqrt{u^2 + v^2}$. Thus, the hydrostatic pressure terms only play a role in the advective flux of energy. Otherwise energy is put into the system by wind stress and taken out by bottom stress. Note that inclusion of the Coriolis terms in (5.8) and (5.9) would not effect the result (5.11) since they do no work.

The response of the ocean to tropical cyclone wind stress is highly rotational, and the kinetic energy exceeds the potential energy by several orders of magnitude (e.g., Tang and Grimshaw 1995). Hence this energy does not propagate very quickly and can be considered trapped within the domain for the timescale on which we make the quasi-steady hypothesis. Thus, the

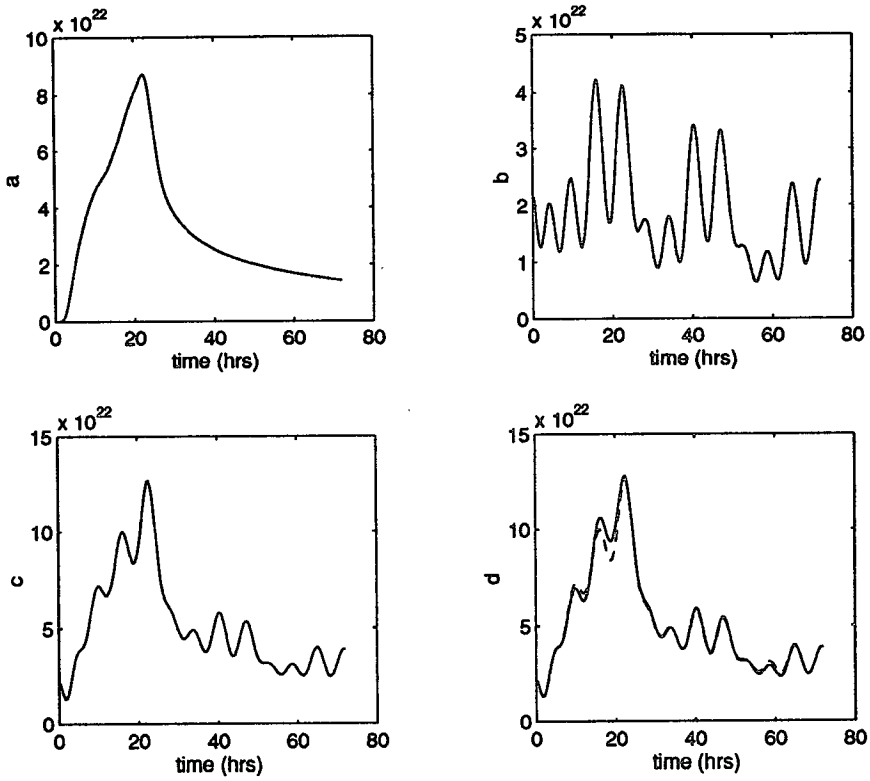


FIG. 6. Plot of total energy $E$: (a) $E_S$ produced by tropical cyclone forcing alone, (b) $E_T$ produced by tidal forcing alone, (c) $E_{TS}$ produced by tropical cyclone forcing and tidal forcing combined, and (d) solid line is the sum of the results $E_S + E_T$ in (a) and (b) and dashed line is the result $E_{TS}$ in (c).

amplitude response is essentially just a balance between the wind stress and the bottom stress, and this can be represented by a scaling in which $(u, v, \zeta) \propto \sqrt{\tau_W}$. This is just the schematic result $\phi_S = \sqrt{F_S}$ obtained above in (5.2). We note that Proctor and Wolf (1990) carried out an energy budget analysis in a hindcast of a North Sea storm surge, and their results confirm that the primary balance for the storm surge is the terms on the right-hand side of (5.11). But, they did not obtain the dimensional result (5.13) below.

For the case of tidal forcing, there is clearly a flux of energy, $E_B$, through the boundary of our computational domain that is balanced by bottom stress. This leads to the scaling relationship $(u, v, \zeta) \propto \sqrt{E_B}$, where now $E_B$ is just the left-hand side of (5.11) evaluated at a representative boundary point. This is the analogue of the schematic result $\phi_T = \sqrt{F_T}$ in (5.2).

Then, for the case of combined tropical cyclone and tidal forcing we obtain the result (5.4) above, which we now see is a global energy balance between forcing and bottom friction. Indeed, this argument can now be carried further since we note that (5.2) can be rewritten in the form

$$\phi_{TS}^2 = \phi_T^2 + \phi_S^2. \tag{5.12}$$

But, since $\phi$ is in fact composed of three quantities, $\zeta$, $u$ and $v$, the expression (5.12) can be interpreted to imply that

$$E_{TS} = E_T + E_S, \tag{5.13}$$

where $E$ is the energy density $\{\frac{1}{2}h(u^2 + v^2) + \frac{1}{2}g\zeta^2\}$ evaluated at each instant of time and then integrated over the whole domain. We plot $E$ in Fig. 6 for the simulation shown in Fig. 3, and the validity of (5.13) is striking.

Given that many different functional forms have been used for bottom friction [ for example, Snyder et al. (1979) use a combination of a linear and a quadratic bottom friction law, while Signell et al. (1990) and Davies and Lawrence (1994) use a parameterization that includes the effects of wind wave turbulence], it is convenient to generalize the results (5.6) and (5.12) in the following way. If we assume that the friction depends on the variable $\phi$ through the functional form $\tau = f(\phi)$, then the following relationship will hold in place of (5.12):

$$f(\phi_{TS}) = f(\phi_T) + f(\phi_S). \tag{5.14}$$

The arguments described above do not account for the relative phase difference at any specific location

between the peak sea level due to the storm surge and that associated with the tide. In practice, there will exist such phase differences imposed a priori by the different phase of the tropical cyclone forcing vis-à-vis the tide, and these could well prevent a strict quantitative application of formulas such as (5.4) or (5.12) at any specific location. Further, the local energy fluxes that occur in the domain and are represented by the left-hand side of (5.11) may prevent the quasi-steady scaling implied by the right-hand side of (5.11), and hence again we cannot generally expect results such as (5.4) or (5.12) to hold universally in space and time. However, such local phase differences are likely to be smoothed out and are relatively unimportant in computing the total energy in formula (5.13). Indeed, this is what we find and the verification of (5.13) shown in Fig. 6 is confirmed when the formula is tested for other parameter settings. Thus, we can infer that the result (5.12) is very robust on average, even if there is some variability due to local phase differences between the storm surge and the tide.

Further, we note that although the quadratic bottom friction does cause a strong interaction between the amplitudes of the storm surge and the tides, there is very little observed phase shift due to this interaction (compare Figs. 3a and 3b with 3c for instance). This can be attributed to the great disparity between the speed of long gravity waves, through which the tides might be expected to adjust to an interaction with the storm surge, and the speed of the tropical cyclone forcing. Also, we note that although the quadratic bottom stress law (2.8) is quadratic in the velocity amplitudes, it is linear in their phases.

Next we note that the present results rely on the use of the quadratic bottom friction law (2.8). In practice this law is sometimes modified to take more account of bottom boundary-layer dynamics. For instance, this law needs to be altered in the nearshore region due to the enhanced friction caused by increased turbulence due to wind-generated surface waves (Grant and Madsen 1979, 1986; Signell et al. 1990; Davies and Lawrence 1994; Tang and Grimshaw 1996b). The incorporation of this effect into the present numerical model is currently under investigation, but in the present context the net outcome of this, or other modifications, can be regarded as replacing the quadratic dependence of $\tau$ on $\phi$ by a more general function form $\tau = f(\phi)$. But then the relation (5.14) replaces (5.12). Further, if, as is likely, $f(\phi)$ is a convex function of $\phi$ just as $\phi^2$ is, then we will again obtain the same basic result (5.4). Hence we argue that this result (5.4) has wide applicability and is largely independent of model parameterizations.

Finally, we point out that our results suggest that a safe and reliable, although overly conservative, method of predicting coastal sea levels due to storm surges in the presence of high tides is to simulate the storm surge alone and then add the astronomical tide, since, on average, this will give an overestimate of sea level. Alternatively, the quantitative dynamical scaling relation (5.12) could be used as a basis for evaluating the amount of overestimate. Of course, it would be preferable to simulate the storm surge and tide together. While this is obviously feasible in hindcast studies or process studies such as the present, in operational forecast simulations it requires an accurate prediction of the location of the wind stress field, and also its relative phase vis-à-vis the tidal forcing, for the duration of the simulation. For storm surges generated by tropical cyclones, the required level of accuracy for these cyclone parameters is presently not usually available.

*Acknowledgments.* We thank Bill Mitchell of the Australian National Tide Facility for supplying tidal information. We acknowledge the support of the National Greenhouse Advisory Committee, DEST, for this project.

## REFERENCES

Andrews, J. C., and L. Bode, 1988: The tides of the central Great Barrier Reef. *Contin. Shelf Res.*, **8,** 1057–1085.

Blumberg, A. F., and G. L. Mellor, 1987: A description of a three-dimensional coastal ocean circulation model. *Three-Dimensional Coastal Ocean Models,* N. S. Heaps, Ed., *Coastal and Estuarine Sciences,* Vol. 4, Amer. Geophys. Union, 1–16.

Csanady, G. T., 1984: *Circulation in the Coastal Ocean.* D. Reidel, 279 pp.

Das, P. K., 1994: Prediction of storm surge in the Bay of Bengal. Kalpathi Ramakrishna Ramanathan Medal Lecture—1993. *Proc. Indian Natl. Sci. Acad. Part A,* **60,** 513–533.

Davies, A. M., and J. E. Jones, 1992: A three-dimensional wind driven circulation model of the Celtic and Irish Seas. *Contin. Shelf Res.,* **12,** 159–188.

——, and ——, 1993: On improving the bed stress formulation in storm surge models. *J. Geophys. Res.,* **98,** 7023–7038.

——, and J. Lawrence, 1994: Examining the influence of wind and wind wave turbulence on tidal currents, using a three-dimensional hydrodynamic model including wave–current interaction. *J. Phys. Oceanogr.,* **24,** 2441–2460.

Fandry, C. B., 1981: Development of a numerical model of tidal and wind-driven circulation in Bass Strait. *Aust. J. Mar. Freshwater Res.,* **32,** 9–29.

Flather, R. A., 1994: A storm surge prediction model for the northern Bay of Bengal with application to the cyclone disaster in April 1991. *J. Phys. Oceanogr.,* **24,** 172–198.

Frank, W. M., 1984: A composite analysis of the core of a mature hurricane. *Mon. Wea. Rev.,* **112,** 2401–2420.

Grant, W. D., and O. S. Madsen, 1979: Combined wave and current interaction with a rough bottom. *J. Geophys. Res.,* **84,** 1797–1808.

——, and ——, 1986: The continental-shelf bottom layer. *Annu. Rev. Fluid. Mech.,* **18,** 265–305.

Heaps, H. S., 1983: Storm surges, 1967–1982. *Geophys. J. Roy Astron. Soc.,* **74,** 331–376.

Holland, G. J., 1980: An analytic model of the wind and pressure profiles in hurricanes. *Mon. Wea. Rev.,* **108,** 1212–1218.

Hubbert, G. D., G. J. Holland, L. M. Leslie, and M. J. Manton, 1991: A real-time system for forecasting tropical cyclone storm surges. *Wea. Forecasting,* **6,** 86–97.

Johns, B., A. D. Rao, S. K. Dube, and P. C. Sinha, 1985: Numerical modelling of tide-surge interaction in the Bay of Bengal. *Philos. Trans. Roy Soc. London, Ser. A,* **313,** 507–535.

Lourensz, R. S., 1981: Tropical cyclones in the Australian region July 1909 to June 1980. Met. Summary, 94 pp. [Available from

Bureau of Meteorology, PO Box 1289K, Melbourne, Vic 3001, Australia.]

Middleton, J. H., V. T. Buchwald, and J. M. Huthnance, 1984: The anomalous tides near Broad Sound. *Contin. Shelf Res.*, **4,** 359–381.

O'Connor, W. P., 1991: A numerical model of tides and storm surges in the Rio de la Plata Estuary. *Contin. Shelf Res.*, **11,** 1491–1508.

Prandle, D., and J. Wolf, 1978: The interaction of surge and tide in the North Sea and River Thames. *Geophys. J. Roy Astron. Soc.*, **55,** 203–216.

Proctor, R., and R. A. Flather, 1988: Storm surge prediction in Bristol Channel—The flood of 13 December 1981. *Contin. Shelf Res.*, **9,** 889–918.

——, and ——, 1990: An investigation of the storm surge of February 1, 1983 using numerical models. *Modeling Marine Systems,* A. M. Davies, Ed., Vol. 1, CRC Press, 43–72.

Sanderson, B. G., A. Okubo, I. T. Webster, S. Kioroglou, and R. Appeldoorn, 1995: Observations and idealized models of dispersion on the southwestern Puerto Rican insular shelf. *Math. Comput. Modelling,* **2,** 39–63.

Signell, R. P., R. C. Beardsley, H. C. Graber, and A. Capotondi, 1990: Effect of wave–current interaction on wind-driven circulation in narrow, shallow embayments. *J. Geophys. Res.*, **95,** 9671–9678.

Smith, S. D., and E. G. Banke, 1975: Variation of the sea surface drag coefficient with wind speed. *Quart. J. Roy. Meteor. Soc.*, **101,** 665–673.

Snyder, R. L., M. Sidjabat, and J. H. Filloux, 1979: A study of tides, setup and bottom friction in a shallow semi-enclosed basin. Part II: Tidal model and comparison with data. *J. Phys. Oceanogr.*, **9,** 170–188.

Tang, Y., 1994: Numerical studies of the coastal ocean. Ph. D thesis, Monash University, 173 pp. [Available from Monash University, Clayton, Victoria 3168, Australia.]

——, and R. Grimshaw, 1995: A modal analysis of the coastally trapped waves generated by tropical cyclones. *J. Phys. Oceanogr.*, **25,** 1577–1598.

——, and ——, 1996a: Radiation boundary conditions in barotropic coastal ocean numerical models. *J. Comput. Phys.*, **123,** 96–110.

——, and ——, 1996b: The effect of wind wave-enhancement of bottom stress on the circulation induced by tropical cyclones on continental shelves. *J. Geophys. Res.*, in press.

——, W. Sun, and S. Feng, 1990a: Numerical modelling of storm surge of Bohai Bay (in Chinese). *Acta Ocean. Sin.*, **12,** 149–159.

——, ——, and ——, 1990b: A method of separating current of the three-dimensional shallow water hydrodynamical model. *Storm Surges: Observations and Modelling, Proc. Int. Symp. on Storm Surge,* J. Chao, T. S. Murty, C. Bao, M. I. El-Sabh, and F. Liu, Eds., 49–60.

Verboom, G. K., J. G. De Rorde, and R. P. Van Dijk, 1992: A fine grid tidal flow and storm surge model of the North Sea. *Contin. Shelf Res.*, **12,** 213–233.

Welander, P., 1961: Numerical prediction of storm surges. *Advances in Geophysics,* Vol. 8, Academic Press, 315–378.

Whittingham, H. E., 1958: The Bathurst Bay Hurricane and associated storm surge. *Aust. Meteor. Mag.*, **23,** 14–36.